International Journal of Nanomedicine

Dovepress

open access to scientific and medical research

Open Access Full Text Article

ORIGINAL RESEARCH

Physicochemical properties, cytotoxicity, and antimicrobial activity of sulphated zirconia nanoparticles

This article was published in the following Dove Press journal:
International Journal of Nanomedicine
19 January 2015
Number of times this article has been viewed

Ae Mftah[1]
Fatah H Alhassan[2,3]
Mothanna Sadiq Al-Qubaisi[4]
Mohamed Ezzat El Zowalaty[4]
Thomas J Webster[5,6]
Mohammed Sh-eldin[7]
Abdullah Rasedee[8]
Yun Hin Taufiq-Yap[2,3]
Shah Samiur Rashid[1]

[1]Department of Chemistry, Faculty of Industrial Sciences and Technology, University Malaysia Pahang, Malaysia; [2]Catalysis Science and Technology Research Centre, [3]Department of Chemistry, Faculty of Science, Universiti Putra Malaysia, Selangor, Malaysia; [4]Institute of Bioscience, University Putra Malaysia, Serdang, Selangor, Malaysia; [5]Department of Chemical Engineering, Northeastern University, Boston, MA, USA; [6]Center of Excellence for Advanced Materials Research, King Abdulaziz University, Jeddah, Saudi Arabia; [7]Solar Energy Research Institute, University Kebangsaan Malaysia, Selangor, [8]Faculty of Veterinary Medicine, Universiti Putra Malaysia, Selangor, Malaysia

Correspondence: Yun Hin Taufiq-Yap
Catalysis Science and Technology Research Centre, Faculty of Science-Universiti Putra Malaysia, 43400 UPM Serdang Selangor, Malaysia
Tel +60 3 8946 6809
Fax +60 3 8946 6758
Email abuohamid9090@gmail.com; taufiq@upm.edu.my

Abdullah Rasedee
Faculty of Veterinary Medicine, Universiti Putra Malaysia, 43400 UPM Serdang, Selangor, Malaysia
Tel +60 3 8946 3455
Fax +60 3 8946 1971
Email rasedee@vet.upm.edu.my

Abstract: Nanoparticle sulphated zirconia with Brønsted acidic sites were prepared here by an impregnation reaction followed by calcination at 600°C for 3 hours. The characterization was completed using X-ray diffraction, thermal gravimetric analysis, Fourier transform infrared spectroscopy, Brunner-Emmett-Teller surface area measurements, scanning electron microscopy with energy dispersive X-ray spectroscopy, and transmission electron microscopy. Moreover, the anticancer and antimicrobial effects were investigated for the first time. This study showed for the first time that the exposure of cancer cells to sulphated zirconia nanoparticles (3.9–1,000 μg/mL for 24 hours) resulted in a dose-dependent inhibition of cell growth, as determined by (4,5-dimethylthiazol-2-yl)-2,5-diphenyltetrazolium bromide assays. Similar promising results were observed for reducing bacteria functions. In this manner, this study demonstrated that sulphated zirconia nanoparticles with Brønsted acidic sites should be further studied for a wide range of anticancer and antibacterial applications.

Keywords: sulphated zirconia, nanoparticles, antimicrobial, anticancer

Introduction

Previously, a number of organic synthesis methods have been carried out with heterogeneous solid acids, leading to better regio- and stereoselectivity.[1–3] It has been found that it is not just the strength of the acid but also the type of acidity (Brønsted or Lewis) that matters for improved activity and selectivity. The inclusion of superacidity in solids has attracted great attention.[4] Among superacid nanoparticles, sulphated zirconia has found several applications and holds large promise in a number of reactions of importance, which would only increase if synthesized into nanoparticles.[5] The activity of nanoparticle sulphated zirconia depends on the successful inclusion of sulphoxy moieties into the zirconium oxide skeleton.[6] Such materials show excellent performance toward α-pinene isomerization in a moderate setting.[7] Production of the drug itself in nanoparticulate form has also been introduced as an approach for the increased release of hydrophobic drugs because of their distinctive advantages over colloidal drug carriers.[8]

In general, metal oxides have been used widely either as such or as supports in conjunction with other active components for many oxidation, reduction, and acid-base-catalyzed reactions.[9–12] For instance, nearly all developed catalysts use an oxide as the energetic phase, which reveals both proton and electron transfer capacities and could be used as a catalyst in neutralization as well as in reduction-oxidation reactions. These metal oxide redox properties are employed in catalytic decontamination schemes for the total oxidation of contaminated constituents.[13–20] The metal oxide scheme with

intrinsic redox features has also been used for discriminatory oxidation of organic materials and to produce vital fine chemicals, such as acids, nitriles, and aldehydes.[21–23]

The surface nature of the metal oxides has been considered advantageous in discerning organic conversions. Because the rate-determining step on the surface of the catalyst can be determined by the density of active centers and surface area, improved enhancers should have high surface area and smaller sizes of particles. Therefore, in the developing field of nanotechnology, the production of metal oxide nanoparticles has received considerable attention because of the unique physicochemical characteristics obtained for nano-sized compared with micron (or conventional)-sized particles.[24,25]

The surface of zirconium oxide is known to possess all of these catalytic activities. Zirconium oxide, or zirconia, when modified with anions such as sulphate ions, gives a highly acidic or superacidic catalyst that has superior activity to catalyze many reactions.[26–28] Zirconia has been widely used to catalyze many engineering reactions.[29,30] Thus, sulphated zirconia and modified sulphated zirconia form an important class of catalysts, as is evident from the large amount of research that has become visible during the past decade.[31] Furthermore, these catalysts show a promising future, in that they can offer environmentally clean routes for the chemical and pharmaceutical industries into the next millennium.

Despite their potential biomedical applications, very few studies have reported on the role of zirconia nanoparticles as anticancer materials. As far as the authors know, this is the first report of the in vitro anticancer effect of sulphated zirconia nanoparticles against three cancer cell lines. Specifically, the toxicity of sulphated zirconia nanoparticles against human colon cancer HT29, human breast cancer MCF-7 and human liver cancer HepG2 cell lines was assessed, showing promising results.

Moreover, it is reported here that these novel nanoparticles hold promise not just for anticancer applications but also for anti-infection applications. The steady increase in the antimicrobial resistance of microorganisms represents a great public health concern. This requires the search for new unconventional antimicrobial agents. Nanotechnology provides promising materials to fight infectious diseases such as nanoparticles with antimicrobial activities. In the present study, the antimicrobial properties of the as-synthesized sulphated zirconia nanoparticles were determined using the agar diffusion method against different Gram-positive and Gram-negative bacteria of clinical significance.

A survey of the literature has also demonstrated that no previous work has been done so far on the investigation of anticancer and antimicrobial effects of sulphated zirconia nanoparticles. The main purpose of this study was to prepare sulphated zirconia superacidic nanoparticles for use as a chemotherapeutic agent against human colon cancer HT29, human breast cancer MCF-7, and human liver cancer HepG2 cell lines. Moreover, the antimicrobial activity of sulphated zirconia nanoparticles against *Candida albicans* was also examined. The sulphated zirconia nanoparticles were prepared by an impregnation method and characterized using X-ray diffraction (XRD), thermal gravimetric analysis (TGA), Fourier transform infrared spectroscopy (FT-IR), Brunner-Emmett-Teller (BET), scanning electron microscopy with energy dispersive X-ray spectroscopy (SEM-EDS), and transmission electron microscopy (TEM).

Experimental

Materials

Ammonium sulphate, zirconium oxy nitrate, and ammonium hydroxide (28%–30%) were obtained from Sigma-Aldrich (St Louis, MO, USA). A trypsin/ethylenediamine tetraacetic acid solution was purchased from Invitrogen (Carlsbad, CA, USA). Dimethylsulfoxide, phosphate-buffered saline, 3-(4,5-dimethylthiazol-2-yl)-2,5-diphenyltetrazolium bromide (MTT), and Dulbecco's Modified Eagle's Medium were purchased from Sigma-Aldrich.

Preparation of the sulphated zirconia nanoparticles

A schematic representation of the preparation of sulphated zirconia nanoparticles is shown in Figure 1.

Physicochemical characterization of sulphated zirconia

Powder XRD analysis was carried out using a Shimadzu diffractometer model XRD 6000. The diffractometer employing Cu-K_α radiation was used to generate diffraction patterns from powder crystalline samples at ambient temperature. The Cu-K_α radiation was generated by a Philips glass diffraction X-ray tube broad focus at 2.7 kW. The crystallite size D of the samples was calculated using the Debye-Scherrer's relationship:[32–34]

$$D=0.9\lambda/(\beta \cos \theta),$$

where D is the crystallite size, λ is the incident X-ray wavelength, β is the full width at half-maximum, and θ is the diffraction angle.

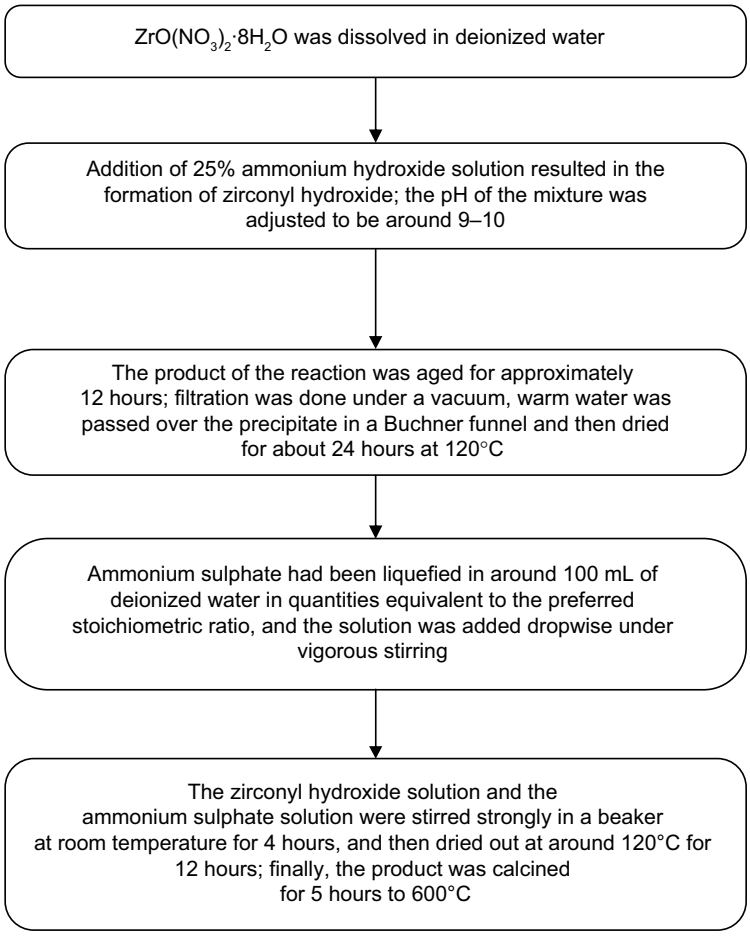

Figure 1 Flow chart for preparation of sulphated zirconia nanoparticles via impregnation method.

The TGA analysis was carried out on a Mettler Toledo Thermo-Gravimetric-Simultaneous Differential Thermal Analysis, Platinum and Rhodium apparatus (Pt crucibles, Pt/Pt–Rh thermocouple) with the purge gas (nitrogen) flow rate of 30 mL minute^{-1} and a heating rate of 10°C minute^{-1} from room temperature to 1,000°C.

Fourier transform infrared analysis was carried out with a PerkinElmer spectrometer model 100 series (sample preparation Universal Attenuated Total Reflectance).

SEM-EDS was used to obtain information about the morphology and chemical composition of the samples. The morphology study of the nanoparticles was carried out using a JEOL scanning electron microscope model JSM-6400, whereas the quantitative chemical composition of the prepared ferric-manganese promoted sulphated zirconia acid catalyst was characterized using EDS for elemental chemical analysis.

TEM (Hitachi H-7100, Japan) was also used to examine the crystal shape. For TEM analysis, the powder was dispersed in deionized water, dropped onto carbon-cover copper grids placed on filter paper, and dried at room temperature.

The zeta potential of the sulphated zirconia nanoparticle dispersions (1 µg of sulphated zirconia nanoparticles dispersed in 1 mL ultradeionized water) were characterized using a ZetaSizer Nano ZS (Malvern Instruments Ltd, Malvern, UK) with dynamic light scattering.

The total surface area of the nanoparticles was obtained using a BET method with nitrogen adsorption at −196°C. Analysis was conducted using a Thermo Fisher Scientific S.P.A. nitrogen adsorption-desorption analyzer (SURFER ANALYZER).

Cell culture

The following human cell lines were obtained from the American Type Culture Collection (Manassas, VA, USA) and were used in the study: human breast cancer (MCF-7), human colon cancer (HT29), human liver cancer (HepG2), and normal human breast (MCF-10a) cells, which were all characterized as virus-negative. They grow as an adherent monolayer of tightly knit epithelial cells. These cells were grown in Dulbecco's Modified Eagle's Medium, which was

supplemented with 10% fetal bovine serum. The media contained penicillin (100 U/mL) and streptomycin (100 g/mL). The cells were grown at 37°C in a humidified 5% CO_2 incubator.

Cytotoxicity MTT assay

HT29, MCF-7, MCF-10a, and HepG2 cells lines were plated at 1×10^3 cells/well by adding 200 µL of a 5×10^3 cells/mL suspension to each well of a 96-well tissue culture plate. The plates were incubated for sufficient time to ensure attachment at 30%–40% confluence. The media was aspirated off and replaced with fresh media (200 µL) containing sulphated zirconia nanoparticles at different concentrations (3.9–250 µg/mL) and chemotherapeutic agents at 0.156–10.0 µg/mL (oxaliplatin for HT29 cells, doxorubicin for both MCF-7 and MCF-10a cells, and tamoxifen for HepG2 cells). The last row was left as an untreated control. The plates were incubated at 37°C, 5% CO_2, for 24 hours. After incubation with the compounds, the media was aspirated off and the cells were washed by phosphate-buffered saline buffer three times to ensure all drugs were removed, and then the buffer was replaced with fresh media. The MTT solution (20 µL) at a total volume of 200 µL was added to every well and mixed gently with the media, which was later incubated for 4–6 hours at 37°C with 5% CO_2. The MTT-containing medium was then removed carefully and replaced with dimethylsulfoxide (200 µL per well) to dissolve the formazan crystals. The plates were read in a microtiter plate reader at 570 nm. The concentration of drug needed to inhibit cell growth by 50% (IC_{50}) was generated from the dose-response curves for each compound and each cell line.

In vitro antimicrobial susceptibility test

Four bacterial strains were used to determine the antibacterial activity for the synthesized sulphated zirconia nanoparticles: two Gram-positive bacteria (methicillin-resistant *Staphylococcus aureus* and *Bacillus subtilis*) and two Gram-negative bacteria (*Salmonella choleraesuis* and *Pseudomonas aeruginosa*). In addition, the yeast *Candida albicans* was used to screen the antifungal activity of the synthesized nanoparticles. The microorganisms were obtained from the microbial culture collection unit, Institute of Bioscience, University Putra Malaysia. The bacterial cultures were maintained on Mueller Hinton agar slants (Sigma-Adrich). The bacterial cultures were incubated overnight in 5 mL Mueller Hinton broth (Sigma-Aldrich) in a Certomat BS-T incubation shaker (Sartorius Stedim Biotech, Aubagne, France) at 37°C and 150 rpm until the culture reached an optical density of 600 of 1.0 (Spekol UV VIS 3.02, Analytic Jena, Jena, Germany), which corresponds to 10^8 colony-forming units per ml.

The antimicrobial activities of the synthesized sulphated zirconia nanoparticles were evaluated against the abovementioned microorganisms, using the agar diffusion (cup diffusion) method according to the guidelines of the Clinical and Laboratory Standards Institute. In brief, 20 mL liquid-autoclaved Mueller Hinton agar (pH 7.3±0.2 at 25°C) was poured onto the disposable sterilized Petri dishes and solidified. The solidified agar plate surfaces were dried in an incubator before streaking of the microorganisms onto the surface of the agar plate. Next, 100 µL of the microbial suspensions in the Mueller Hinton broth was streaked over the dried surface of the agar plates and spread uniformly, using a sterilized glass rod. The plates were then dried. Wells were then created in the agar plates, using a sterilized cork borer; the wells were filled with the nanoparticle suspensions in distilled water; and the control wells were filled with ampicillin (for Gram-negative bacteria), streptomycin (for Gram-positive bacteria), and nystatin (for *Candida albicans*) solutions as controls. The experiment was performed in triplicate, and the diameters of the zone of inhibition were measured to the nearest millimeter, using a caliper after a 24-hour incubation at 37°C. Differences between means were determined using standard analysis of variance, followed by Student *t*-tests.

Results and discussion

Figure 2 shows the thermogravimetric curve of sulphated zirconia, and the mass losses found from the TGA measurements agreed fairly well with those expected for the decomposition of hydrated sulphated zirconia.[35] Therefore, the heating events for this sample below 620°C are attributed

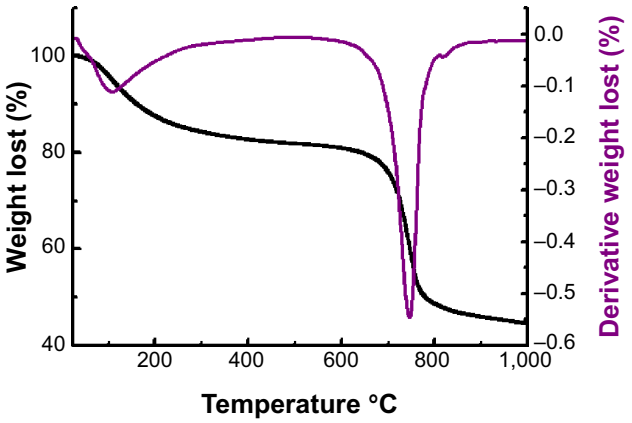

Figure 2 Thermogravimetric curve of sulphated zirconia calcined at 600°C for 3 hours.

to the removal of adsorbed water and the dehydroxylation process of $ZrO(OH)_2$, whereas the second major weight loss at a higher temperature began at about 673°C and ended at 926°C and is referred to as the decomposition of sulphate groups.[36]

Figure 3 depicts the Fourier transform infrared spectroscopy spectra of sulphated zirconia from these spectra, and the presence of sulphate groups was confirmed by the band at the range of 1,225–1,070 cm^{-1}, a result of the asymmetric and symmetric stretching frequency of the O=S=O and O–S–O groups.[37,38] The absence of peaks around 1,450 cm^{-1} confirmed the presence of polynuclear sulphate in the sample irrespective of the high sulphate loading. The band around 1,625 crn^{-1} and 3,325 crn^{-1} corresponds to the bending and stretching modes of the –OH groups of water molecules present in the sample. The presence of these bands even after high temperature calcination points to the existence of Brønsted acidity in the samples.

The specific surface area for the sulphated zirconia and zirconia obtained using the BET method was 38.0 and 34.6 m^2/g, respectively. It was also observed that the incorporation of the sulphate dopant in the structure of zirconia caused an increase in specific surface area and pore size of sulphated zirconia. This allowed reactants to be in contact with more acid sites, and the nanoparticles would have better activity.

The powder XRD patterns of sulphated zirconia calcined at 600°C for 3 hours is illustrated in Figure 4. The XRD patterns of sulphated zirconia show peaks assigned to both the tetragonal phase at 2θ (30.2°, 35.4°, 50.2°, 60.3°) (JSPDS file 00-014-0534: zirconium oxide) and diffraction lines around 2θ (43.8°, 62.9°, 75.1°) (JSPDS file 01-086-1449ZrO_2) of the monoclinic phase of zirconia.[1,39] By using the Scherrer's equation, the average size of sulphated zirconia was estimated to be 40 nm.

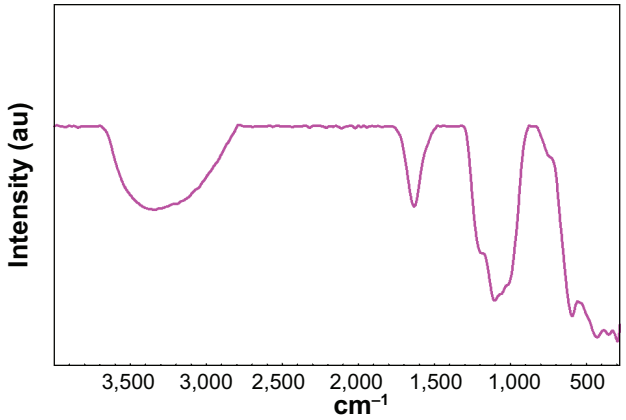

Figure 3 Fourier transform infrared spectroscopy spectra of calcined sulphated zirconia.

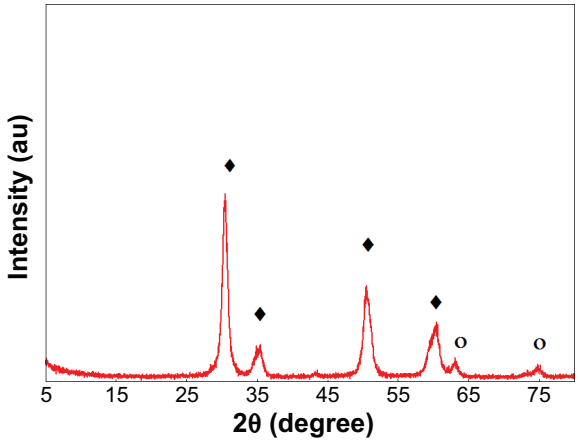

Figure 4 X-ray diffraction patterns of sulphated zirconia calcined at 600°C for 3 hours.
Notes: O, monoclinic phase; ♦, tetragonal phase of zirconia.

The morphology of the sulphated zirconia was studied by SEM. SEM images of zirconia and sulphated zirconia are presented in Figure 5. In contrast with pure zirconia, SEM images of the sulphated zirconia showed a lower agglomeration. This supports the retarding effect of sulphate doping on the prevention of agglomeration via sulphation. EDS was used to analyze the percentage of elements present in the sample.[40,41] The quantitative percentage of sulphated zirconia elements were found to be sulphur, at 1.66%; zirconium, at 51.95%; and oxygen, at 46.39%.

The morphology and the extent of dispersion of our nanoparticles were determined with TEM. The TEM images of pure sulphated zirconia nanoparticles are shown in Figure 6. It is apparent that the nanoparticles are approximately tetragonal in shape, with diameters ranging from 37 to 54 nm, with an average size at 43 nm. In addition, most of the nanoparticles agglomerated, and a few detached.[42,43]

The zeta potential for the sulphated zirconia nanoparticle suspensions was −8.41 mV, as shown in Figure 7. This finding may suggest that sulphated zirconia nanoparticles tend to aggregate in deionized and double-distilled water; their low zeta potential of −8.41 mV indicates these nanoparticles have poor electrostatic repulsion characteristics and are very unstable.

Most important, the cytotoxicity of sulphated zirconia nanoparticles on MCF-7, HT29, HepG2, and MCF-10a cells was determined by MTT assays.[44,45] Figure 8 shows that sulphated zirconia nanoparticles have significant cytotoxic effects against colon cancer HT29 cells at most concentrations tested ($P<0.05$). For the case of both MCF-7 and HepG2 cells, 15.6 µg/mL had no significant effect on cell growth, whereas the nanoparticles inhibited the growth of all cell lines tested

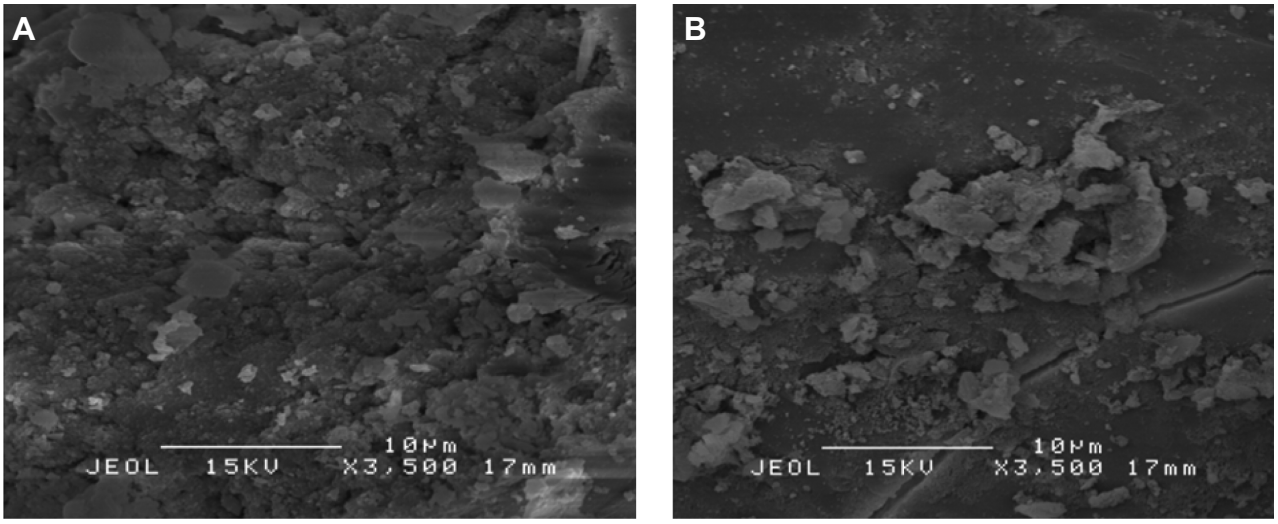

Figure 5 Scanning electron microscopy images of zirconia (**A**) and sulphated zirconia (**B**) calcined at 600°C for 3 hours.

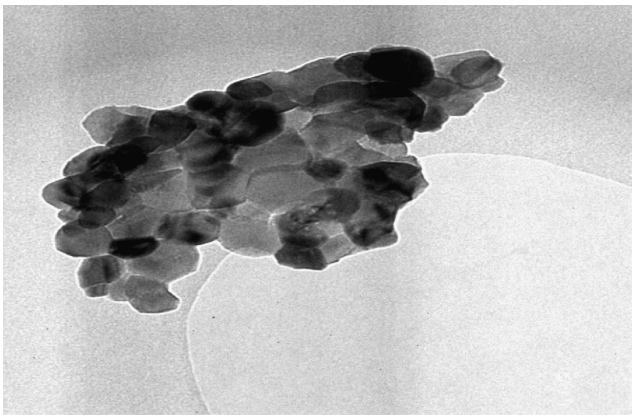

Figure 6 The transmission electron microscopy images of pure sulphated zirconia nanoparticles.

		Mean (mV)	Area (%)	Width (mV)
Zeta potential (mV): –8.41	**Peak 1:**	–8.41	100.0	4.11
Zeta deviation (mV): 4.11	**Peak 2:**	0.00	0.0	0.00
Conductivity (mS/cm): 0.137	**Peak 3:**	0.00	0.0	0.00
Result quality: Good				

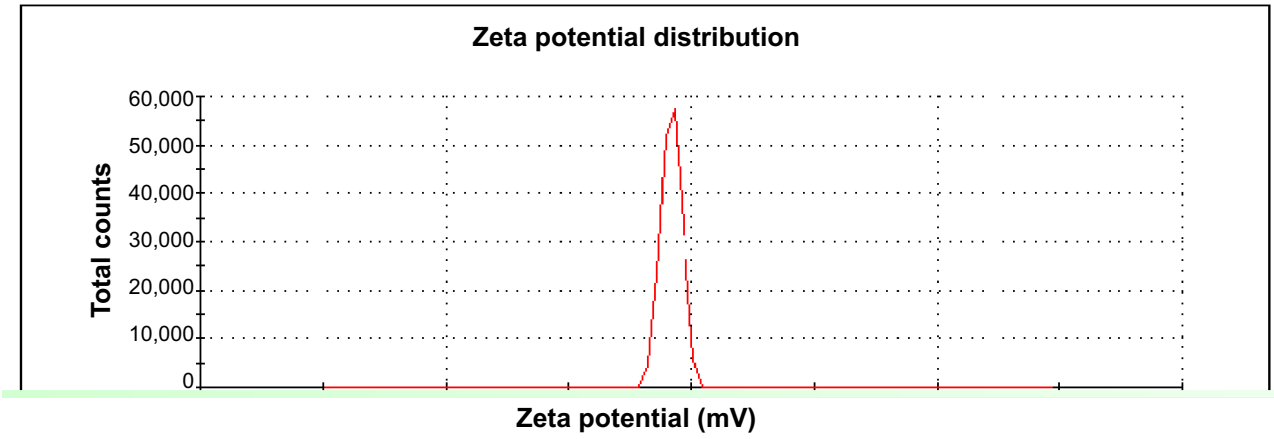

Figure 7 Surface charge characterization of sulphated zirconia nanoparticles.

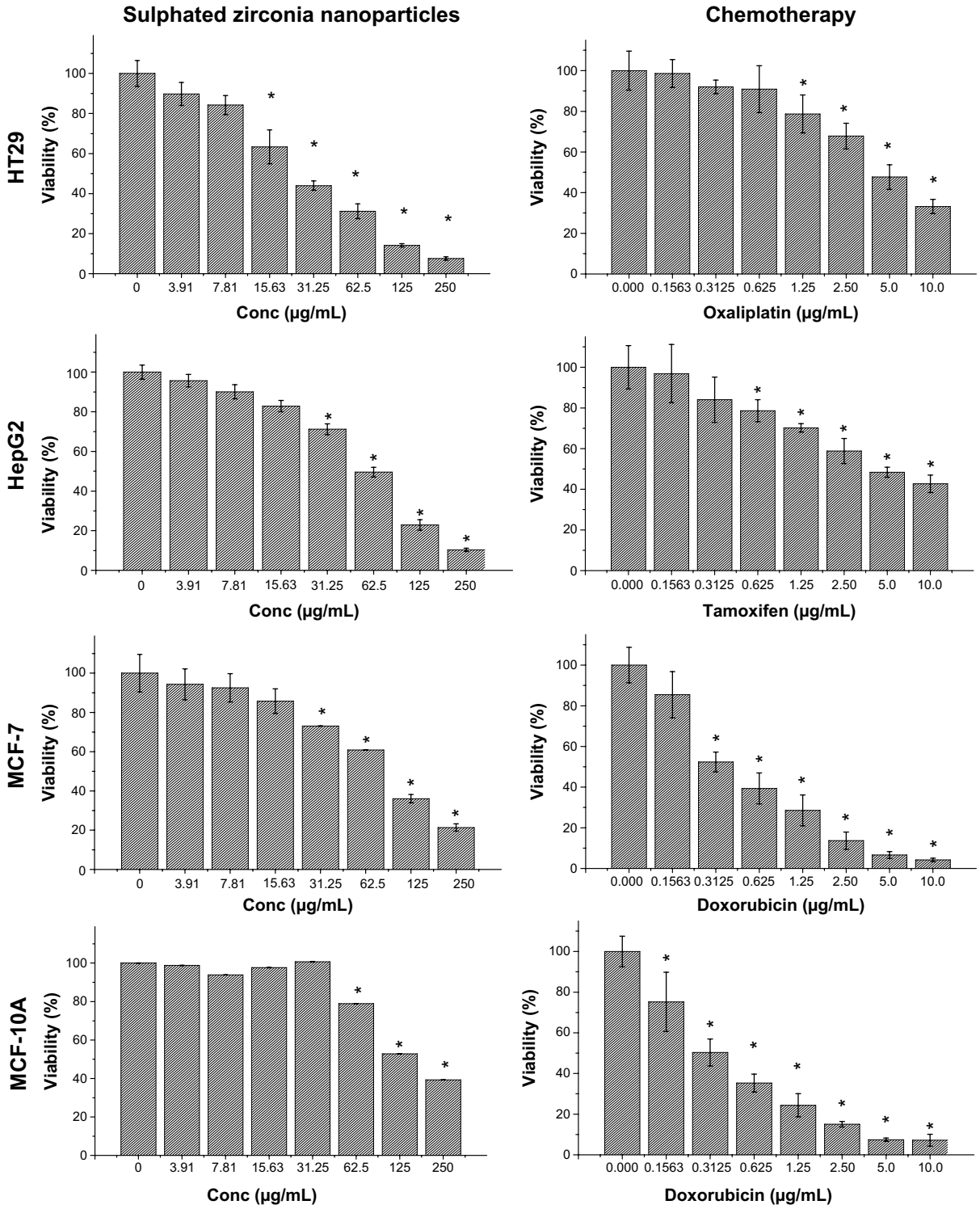

Figure 8 Sulphated zirconia nanoparticles and chemotherapeutic effects on the viability of treated cells, which were evaluated through mitochondrial activity using an (4,5-dimethylthiazol-2-yl)-2,5-diphenyltetrazolium bromide assay.
Notes: Mean ± standard deviation (n=3 wells/treatment). *$P<0.05$ compared with the untreated cells.

in a dose-dependent manner. The IC_{50} values of sulphated zirconia nanoparticles calculated from the dose-response curves are shown in Table 1. In contrast, the normal breast MCF-10a cells were the least sensitive to sulphated zirconia nanoparticles, with an IC_{50} value of approximately 151.6 μg/mL, whereas the breast cancer MCF-7 cells were found to be more sensitive, with an IC_{50} value of 89.9 μg/mL. The IC_{50} value of sulphated zirconia nanoparticles in normal

breast MCF-10a cells was almost 1.7 times higher than that in breast cancer MCF-7 cell lines (Table 1). Furthermore, compared with sulphated zirconia nanoparticles, doxorubicin showed higher cytotoxicity in the normal breast MCF-10a cell line. The results obtained from the MTT assay showed significant changes in the viability of MCF-10a cells treated with nanoparticles at concentrations of 62.5 and 125 µg/mL for 24 hours when compared with untreated cells.

As shown in Figures 9 and 10, the sulphated zirconia nanoparticles showed high antimicrobial activity against both Gram-positive and Gram-negative bacteria. It was found that the nanoparticles showed the highest activity against *Pseudomonas aeruginosa* and methicillin-resistant *S. aureus*, followed by *Bacillus subtilis* and *Salmonella choleraesuis*. In contrast, the sulphated zirconia nanoparticles did not show any activity against *Candida albicans*, suggesting a lack of antifungal activity. Other fungal species may be used to detect any possible antifungal effect of the sulphated zirconia nanoparticles.

All of these microorganisms are responsible for a range of serious infections in human and animal populations.

Table 1 Concentration of drug needed to inhibit cell growth by 50% of sulphated zirconia nanoparticles, oxaliplatin, doxorubicin, and tamoxifen on HT29, MCF-7, MCF-10a, and HepG2

Treatment	Concentration of drug needed to inhibit cell growth by 50%, µg/mL			
	HepG2	HT29	MCF-7	MCF-10a
Nanoparticles	61.8	26.4	89.8	151.63
Tamoxifen	4.62	–	–	–
Oxaliplatin	–	4.71	–	–
Doxorubicin	–	–	0.37	0.32

Note: MCF-10a cells are a normal, healthy cell line.

Therefore, the sulphated zirconia nanoparticles could find various biomedical applications of therapeutic importance to counteract such highly resistant microorganisms. Moreover, these sulphated zirconia nanoparticles should be further studied because of their noted anticancer properties.

Conclusion

The present study showed that sulphated zirconia nanoparticles have significant cytotoxic effects against colon cancer HT29 cells at most concentrations tested and inhibited the

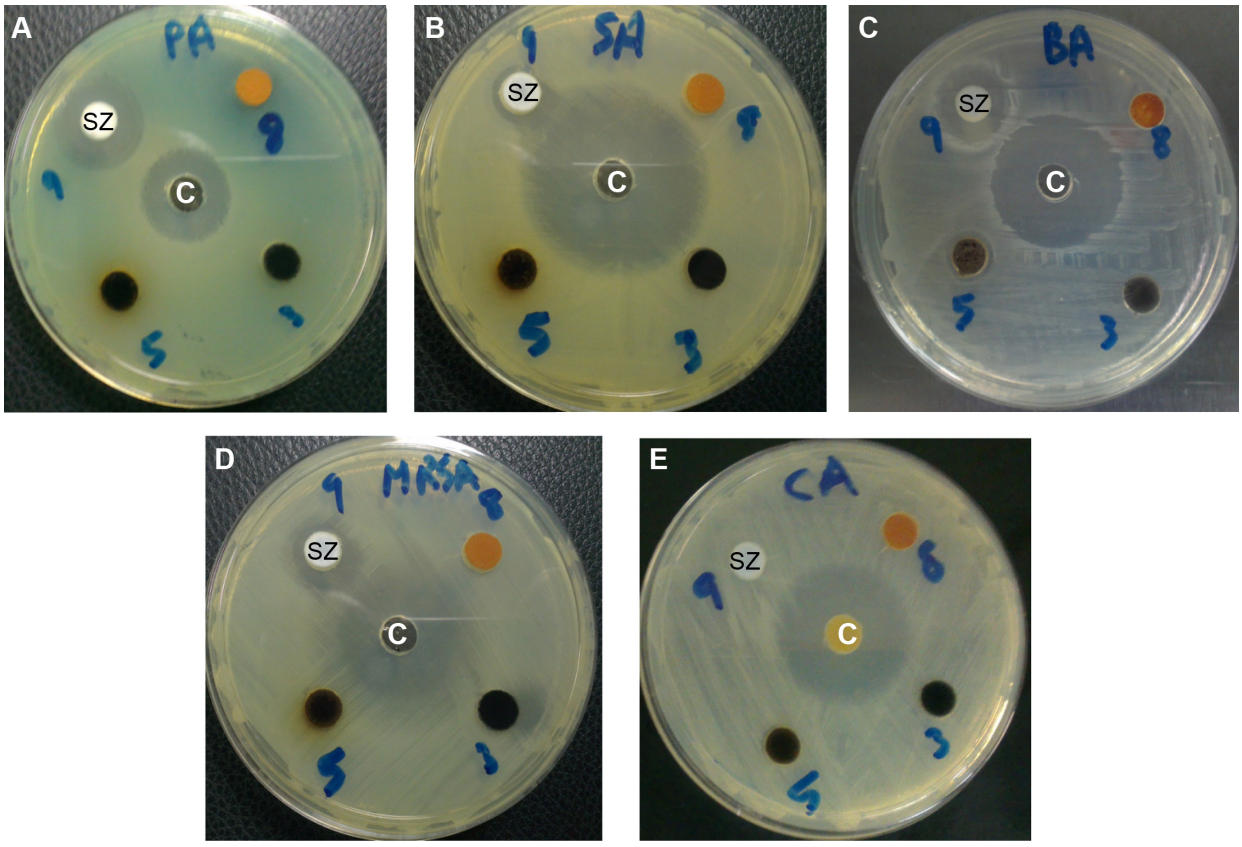

Figure 9 Antimicrobial activity of sulphated zirconia nanoparticles (SZ), against bacteria and yeast, using disk agar diffusion method.
Notes: Photographs of SZ nanoparticles: (**A**) *Pseudomonas aeruginosa*, (**B**) *Salmonella choleraesuis*, (**C**) *Bacillus subtilis*, (**D**) methicillin-resistant *Staphylococcus aureus,* and (**E**) *Candida albicans*. Control antimicrobial agents (**C**) (ampicillin for Gram-negative, streptomycin for Gram-positive, and nystatin for *Candida albicans*).

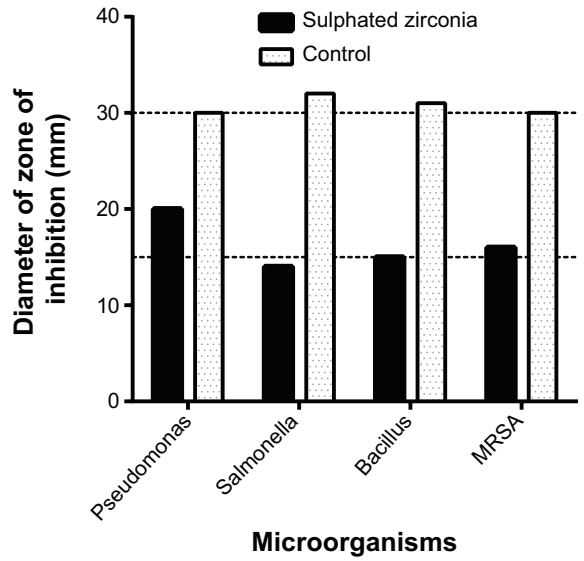

Figure 10 Diameter of zones of inhibition of sulphated zirconia nanoparticles against bacteria and yeast, along with the control antimicrobial agents (ampicillin for Gram-negative, streptomycin for Gram-positive).
Note: For *Candida albicans*, zone was 0 mm, and no activity was reported.

growth of all cancer cell lines studied here. Normal human breast MCF-10a cells exhibited the highest resistance to sulphated zirconia nanoparticles. Furthermore, the sulphated zirconia nanoparticles also showed high antimicrobial activity against both Gram-positive bacteria and Gram-negative bacteria. In conclusion, the sulphated zirconia nanoparticles could find numerous biomedical applications of therapeutic importance to counteract the colon cancer, as well as highly resistant microorganisms.

Disclosure

The authors report no conflicts of interest in this work.

References

1. Jentoft FC, Hahn A, Kröhnert J, et al. Incorporation of manganese and iron into the zirconia lattice in promoted sulfated zirconia catalysts. *J Catal*. 2004;224(1):124–137.
2. Reddy BM, Patil MK. Organic syntheses and transformations catalyzed by sulfated zirconia. *Chem Rev*. 2009;109(6):2185–2208.
3. Yadav GD, Nair JJ. Sulfated zirconia and its modified versions as promising catalysts for industrial processes. *Microporous Mesoporous Mater*. 1999;33(1):1–48.
4. Brown AC, Hargreaves JJ. Sulfated metal oxide catalysts. *Green Chem*. 1999;1(1):17–20.
5. Clark JH. Solid acids for green chemistry. *Acc Chem Res*. 2002;35(9):791–797.
6. Delahay G, Ensuque E, Coq B, Figuéras F. Selective Catalytic Reduction of Nitric Oxide byn-Decane on Cu/Sulfated-Zirconia Catalysts in Oxygen Rich Atmosphere: Effect of Sulfur and Copper Contents. *J Catal*. 1998;175(1):7–15.
7. Ecormier MA, Wilson K, Lee AF. Structure–reactivity correlations in sulphated-zirconia catalysts for the isomerisation of α-pinene. *J Catal*. 2003;215(1):57–65.
8. Date AA, Patravale V. Current strategies for engineering drug nanoparticles. *Curr Opin Colloid Interface Sci*. 2004;9(3–4):222–235.
9. Pissuwan D, Valenzuela SM, Cortie MB. Therapeutic possibilities of plasmonically heated gold nanoparticles. *Trends Biotechnol*. 2006;24(2):62–67.
10. Hafner A, Braese S. Efficient Trifluoromethylation of Activated and Non Activated Alkenyl Halides by Using (Trifluoromethyl) trimethylsilane. *Adv Synth Catal*. 2011;353(16):3044–3048.
11. Thibault-Starzyk F, Stan I, Abelló S, et al. Quantification of enhanced acid site accessibility in hierarchical zeolites–The accessibility index. *J Catal*. 2009;264(1):11–14.
12. Bond GC. *Metal-catalysed reactions of hydrocarbons*. New York; Springer; 2006.
13. Kašpar J, Fornasiero P. Nanostructured materials for advanced automotive de-pollution catalysts. *J Solid State Chem*. 2003;171(1):19–29.
14. Trovarelli A, Zamar F, Llorca J. Leitenburg Cd, Dolcetti G, Kiss JT. Nanophase fluorite-structured CeO2–ZrO2 catalysts prepared by high-energy mechanical milling. *J Catal.* 1997;169(2):490–502.
15. Zhou L, Xu J, Li X, Wang F. Metal oxide nanoparticles from inorganic sources via a simple and general method. *Mater Chem Phys*. 2006;97(1):137–142.
16. Dong S, Han C, Zheng B, Zhang M, Huang F. Preparation of two new [2] rotaxanes based on the pillar [5] arene/alkane recognition motif. *Tetrahedron Lett*. 2012;53(28):3668–3671.
17. Chizallet C, Raybaud P. Pseudo-bridging silanols as versatile Brønsted acid sites of amorphous aluminosilicate surfaces. *Angew Chem Int Ed Engl*. 2009;48(16):2891–2893.
18. Yan J, Yu D, Li H, Sun P, Huang H. NaY zeolites modified by La3+ and Ba2+: the effect of synthesis details on surface structure and catalytic performance for lactic acid to acrylic acid. *J Rare Earths*. 2010;28(5):803–806.
19. Carniti P, Gervasini A, Marzo M. Absence of expected side-reactions in the dehydration reaction of fructose to HMF in water over niobic acid catalyst. *Catal Commun*. 2011;12(12):1122–1126.
20. Kuhn JN, Huang W, Tsung C-K, Zhang Y, Somorjai GA. Structure sensitivity of carbon-nitrogen ring opening: impact of platinum particle size from below 1 to 5 nm upon pyrrole hydrogenation product selectivity over monodisperse platinum nanoparticles loaded onto mesoporous silica. *J Am Chem Soc*. 2008;130(43):14026–14027.
21. Liu C, Wang J, Li Y. One-pot synthesis of 3,4-dihydropyrimidin-2 (1H)-(thio) ones using strontium (II) nitrate as a catalyst. *J Mol Catal Chem*. 2006;258(1–2):367–370.
22. Aghapoor K, Ebadi-Nia L, Mohsenzadeh F, Mohebi Morad M, Balavar Y, Darabi HR. Silica-supported bismuth (III) chloride as a new recyclable heterogeneous catalyst for the Paal–Knorr pyrrole synthesis. *J Organomet Chem*. 2012;708–709:25–30.
23. Zou X-X, Li G-D, Wang Y-N, et al. Direct conversion of urea into graphitic carbon nitride over mesoporous TiO2 spheres under mild condition. *Chem Commun (Camb)*. 2011;47(3):1066–1068.
24. Yan W, Wang R, Xu Z, et al. A novel, practical and green synthesis of Ag nanoparticles catalyst and its application in three-component coupling of aldehyde, alkyne, and amine. *J Mol Catal Chem*. 2006;255(1–2):81–85.
25. Kumar D, Reddy VB, Mishra BG, Rana R, Nadagouda MN, Varma RS. Nanosized magnesium oxide as catalyst for the rapid and green synthesis of substituted 2-amino-2-chromenes. *Tetrahedron*. 2007;63(15):3093–3097.
26. Zhang X, Du AJ, Lee P, Sun DD, Leckie JO. Grafted multifunctional titanium dioxide nanotube membrane: separation and photodegradation of aquatic pollutant. *Appl Catal B*. 2008;84(1–2):262–267.
27. Naik MA, Mishra BG, Dubey A. Combustion synthesized WO3–ZrO2 nanocomposites as catalyst for the solvent-free synthesis of coumarins. *Colloids Surf A Physicochem Eng Asp*. 2008;317(1–3):234–238.
28. Samantaray S, Hota G, Mishra B. Physicochemical characterization and catalytic applications of MoO3–ZrO2 composite oxides towards one pot synthesis of amidoalkyl naphthols. *Catal Commun*. 2011;12(13):1255–1259.
29. Song X, Sayari A. Sulfated zirconia-based strong solid-acid catalysts: recent progress. *Catal Rev*. 1996;38(3):329–412.

30. Katada N, Endo J-i, Notsu K-i, Yasunobu N, Naito N, Niwa M. Superacidity and catalytic activity of sulfated zirconia. *J Phys Chem B*. 2000;104(44):10321–10328.
31. Meghshyam K. *Synthesis of Novel Zirconia Based Solid Superacids Their Characterization and Application in Organic Synthesis and Transformation Reactions* [thesis]. Hyderabad, India: Osmania University; 2009.
32. Alhassan FH, Rashid U, AL-Qubaisi MS, Rasedee A, Taufiq-Yap YH. The effect of sulphate contents on the surface properties of iron-manganese doped sulphated zirconia catalysts. *Powder Technol*. 2014;253:809–813.
33. Al-Qubaisi MS, Rasedee A, Flaifel MH, et al. Cytotoxicity of nickel zinc ferrite nanoparticles on cancer cells of epithelial origin. *Int J Nanomedicine*. 2013;8:2497–2508.
34. Al-Qubaisi MS, Rasedee A, Flaifel MH, et al. Induction of apoptosis in cancer cells by NiZn ferrite nanoparticles through mitochondrial cytochrome C release. *Int J Nanomedicine*. 2013;8:4115–4129.
35. Bi M, Li H, Pan W-P, Lloyd WG, Davis BH. Thermal studies of metal promoted sulfated zirconia. *Am Chem Soc Fuel Div Preprints.* 1996;41:77–81.
36. Khalaf HA. Textural properties of sulfated iron hydroxide promoted with aluminum. *Monatsh Chem.* 2009;140(6):669–674.
37. Clearfield A, Serrette G, Khazi-Syed A. Nature of hydrous zirconia and sulfated hydrous zirconia. *Catal Today*. 1994;20(2):295–312.
38. Mekhemer GAH, Khalaf HA, Mansour SAA, Nohman AKH. Sulfated alumina catalysts: consequences of sulfate content and source. *Monatsh Chem.* 2005;136(12):2007–2016.
39. Yamamoto T, Tanaka T, Takenaka S, et al. Structural analysis of iron and manganese species in iron-and manganese-promoted sulfated zirconia. *J Phys Chem B*. 1999;103(13):2385–2393.
40. Zhang L, Yang J, Zhu J, et al. Properties and liquefaction activities of ferrous sulfate based catalyst impregnated on two Chinese bituminous coals. *Fuel*. 2002;81(7):951–958.
41. Yang L, Zhang A, Zheng X. Shrimp shell catalyst for biodiesel production. *Energy Fuels*. 2009;23(8):3859–3865.
42. Butt H-J, Cappella B, Kappl M. Force measurements with the atomic force microscope: Technique, interpretation and applications. *Surf Sci Rep*. 2005;59(1–2):1–152.
43. Li Y, Somorjai GA. Nanoscale advances in catalysis and energy applications. *Nano Lett*. 2010;10(7):2289–2295.
44. Al-Qubaisi M, Rosli R, Subramani T, et al. Goniothalamin selectively induces apoptosis on human hepatoblastoma cells through caspase-3 activation. *Nat Prod Res*. 2013;27(23):2216–2218.
45. Al-Qubaisi M, Rozita R, Yeap S-K, Omar A-R, Ali A-M, Alitheen NB. Selective cytotoxicity of goniothalamin against hepatoblastoma HepG2 cells. *Molecules*. 2011;16(4):2944–2959.